

## NUMERICAL INVESTIGATIONS OF THE APERTURE SIZE EFFECT FOR MAINTAINING A CONSTANT TEMPERATURE IN A NOVEL SULFUR-AMMONIA WATER SPLITTING CYCLE APPLICATION

by

**Jawad SARWAR<sup>a</sup>, Arun SRINIVASA<sup>b</sup>,  
and Konstantinos KAKOSIMOS<sup>a\*</sup>**

<sup>a</sup> Department of Chemical Engineering, Texas A&M University at Qatar, Doha, Qatar

<sup>b</sup> Department of Mechanical Engineering, Texas A&M University, College Station, Tex., USA

Original scientific paper

<https://doi.org/10.2298/TSCI141220075S>

*Solar-driven thermochemical water splitting cycle is a promising, energy efficient and environmentally friendly approach to produce hydrogen. In this paper, numerical work has been undertaken using a cylindrical solar receiver to investigate fixed and variable aperture sizes to maintain constant steady-state temperature over a day for thermochemical part of a novel hybrid photo-thermochemical sulfur-ammonia cycle. A previously developed and validated optical model in commercial software, TracePro<sup>®</sup> is used to simulate the light sources of 10, 15, and 28 kW. The sunlight intensity variations for the designated reference day for this study is selected as July 1, 2011, at 39.74 N, 105.18 W and at an elevation of 1829 m. A developed and validated finite volume based coupled Monte Carlo, Heat Transfer model is used to calculate the steady-state temperatures in the receiver by utilizing the output of the optical model. The simulations are performed at different aperture diameters from 2 to 14 cm to quantify the effect of fixed aperture size on the steady-state temperatures of the receiver. Furthermore, simulations to maintain steady-state temperatures of 673, 823, and 1123 K for different sub-cycles of the selected cycle via variable aperture has been performed and compared with selected fixed apertures. It is found that the variable apertures can maintain desired constant temperatures over the day for each thermochemical sub-cycle. The comparison of overall power consumption and savings for fixed and variable apertures has also been investigated and reported.*

*Key words: solar thermochemical, finite volume method, Monte Carlo method, heat transfer*

### Introduction

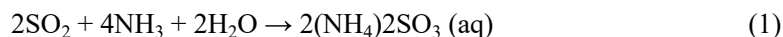
Single step thermal dissociation of water is called water thermolysis. But thermolysis requires temperatures above 2500 K to achieve dissociation [1] and thermodynamic requirements of direct thermal dissociation of water into H<sub>2</sub> and O<sub>2</sub> is difficult to achieve considering structural constraints since the structural material would have to withstand severe thermal conditions [2]. Therefore, the overall solar to hydrogen conversion efficiency of thermolysis is very low [1]. Two-step solar thermochemical water splitting cycle eliminates need for H<sub>2</sub>/O<sub>2</sub> separation. Two-step solar thermochemical water splitting cycles based on metal oxides redox reactions have been proposed *i. e.* Zn, Cd, Fe, Me, Ce oxides, *etc.* The first

\* Corresponding author, e-mail: k.kakosimos@qatar.tamu.edu

step is an endothermic reaction that separates metal from oxygen, while second step involves an exothermic reaction that produces hydrogen and recovers metal oxide for re-use. Several researchers have investigated the two-step ZnO/Zn solar thermochemical cycle. The first step is the endothermic dissociation of the ZnO that produces Zn and oxygen while second step is the exothermic hydrolysis of Zn to produce hydrogen [1, 3-6]. Two-step solar thermochemical water splitting cycles do not utilize the quantum component (*i. e.* visible spectrum of solar energy) which limits the overall solar energy to hydrogen conversion efficiency. Furthermore, it requires significantly higher temperatures (>2000 K) which limits the choice of materials and solar concentrating system. Therefore, multi-step solar thermochemical water splitting cycles have been proposed that utilize photon component of the incident irradiance and require much lower temperatures than the two-step cycle (<1200 K) [7].

A novel multi-step sulfur-ammonia (h-SA) cycle has been proposed by the Florida Solar Energy Centre that uses photon energy (wavelengths >350 nm) to produce hydrogen while thermal energy is used to achieve reversibility of the cycle [7-9]. This new cycle utilizes both visible and infrared part of the solar irradiance thereby achieving higher efficiency as compared to the two-step cycle [10]. Further modifications in this thermochemical step of the sulfur-ammonia cycle have been investigated to avoid the challenge of catalyst deactivation [11]. It is found that the introduction of metal oxides (ZnO) and metal pyro-sulfate (ZnSO<sub>4</sub>, K<sub>2</sub>SO<sub>4</sub>, etc.) instead of water reduces catalyst deactivation. The chemical reactions of the novel h-SA cycle are shown in eqs. (1)-(5):

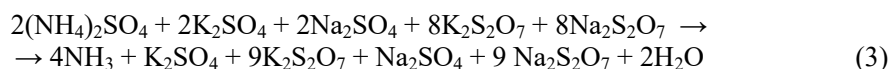
– chemical absorption at 273 K



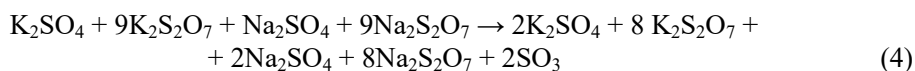
– photochemical at 353 K



– solar thermochemical sub-cycle1 at 673 K



– solar thermochemical sub-cycle2 at 823 K



– solar thermochemical sub-cycle3 at 1123 K



The solar photo catalytic step, shown in eq. (2), is used to generate hydrogen while sub-cycles 1-3 shown in eqs. (3)-(5), produce oxygen and recover ammonia and sulfur dioxide for the chemical absorption reaction shown in eq. (1).

The thermochemical reaction takes place in a reactor utilizing concentrated solar energy to achieve the desired temperature. There are several reactor geometries being investigated by researcher for thermochemical applications. For example, cylindrical cavity – receiver with different flow configurations [12], spherical vessels [13], tube reactors [5], and fluidized bed reactors [14]. The essential part of any reactor is the opening, referred as aperture which allows the irradiance to enter in the reactor. The size of the aperture dictates the optical and re-radiation losses and there exists a trade-off between maximizing irradiance in-

terception and minimizing re-radiation losses. It has been reported that the fixed aperture cannot maintain a constant temperature over a day and variation of up to 190 K is reported [15]. For h-SA cycle, it is essential to control and maintain the temperature of the reactor to achieve reversibility of the cycle.

It has been proposed that a variable aperture can maintain a constant temperature in a reactor and an aperture control device has also been patented [16]. Furthermore, effect of the aperture size on the flux and temperature distribution has been widely studied for methane cracking [17, 18] but no studies has been carried out, so far, for water-splitting application.

Monte Carlo ray tracing method coupled with a finite volume based heat transfer model is a popular tool to investigate the thermal behavior of a reactor, [19-21]. An optical model integrated with a coupled finite volume based Monte Carlo/Heat Transfer has been developed in MATLAB and experimentally validated by author(s), [15]. This validated model forms the basis of this research to investigate the thermal behavior of the solar thermochemical sub-cycles of the novel h-SA cycle. The possibility of maintaining constant temperatures in different sub-cycles of h-SA cycle has been investigated along with optical and power consumption/savings analysis.

## Methodology

### Optical model

A validated optical model, developed by employing TracePro®, is used in this work to simulate the incident irradiance. Preliminary studies have shown that light source of 10, 15, and 28 kW can achieve the receiver temperature required for sub-cycles 1, 2, and 3, respectively. Schematic illustration of the optical model is shown in fig. 1.

The detailed description of the optical model and the characterization of the light source are presented elsewhere [15, 22] but relevant features are discussed here for the sake of clarity. The optical model consists of an elliptical reflector (diameter: 340 mm, first focal point: 55 mm and second focal point: 825 mm apart from first focal point), and a xenon short arc lamp. The arc of the lamp is simulated by a combination of spheres and cylinders assuming a 50% electrical to thermal conversion efficiency.

The power at the arc is assumed as 10, 15, and 28 kW and light emission is considered as Lambertian. The light emitted from the lamp is concentrated on an aperture. Different diameters of the aperture are considered *i. e.* 4, 6, 8, 10, 12, and 14 cm thus, referred as variable aperture. The flux distribution is obtained at selected aperture sizes and power levels using 1 million rays. These rays are referred as primary rays in the subsequent text. The cumulative power incident at the aperture is correlated with a day's irradiance. The selected reference day for this research is July 1, 2011, at latitude and longitude of 39.74 N and 105.18 W, respectively, and at an elevation of 1829 m [23]. The flux distribution at the aperture and comparative power over the day is presented in *Results and discussion*. The obtained flux distribution at the

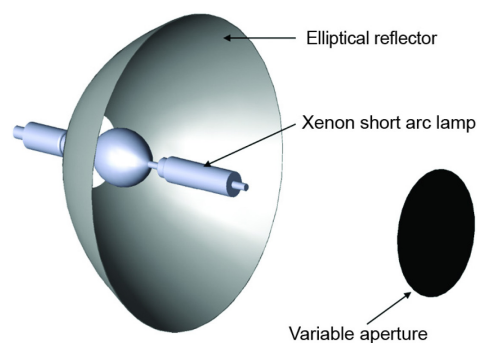
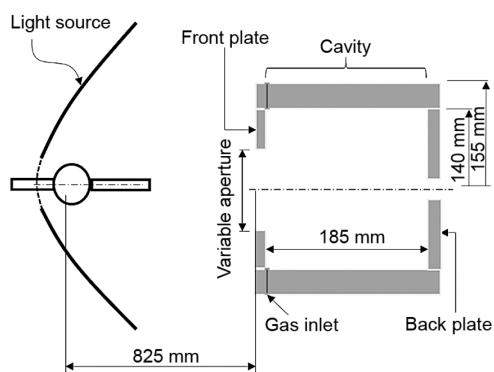


Figure 1. Schematic illustration of the optical model

variable aperture serves as an input to a developed and validated numerical model described in next section.

### Monte Carlo/heat transfer model

The schematic illustration of the light source and a cylindrical receiver is shown in fig. 2. The receiver consists of a front plate, back plate, cavity, aperture, and exhaust. The length of the cavity is 185.5 mm with inner diameter of 140 mm. The thickness of the cavity, front and back plate is considered 15 mm. A quartz window is considered between front plate and the cavity which is assumed perfectly transmitting material. The material of the receiver is considered Inconel (Grade 601).



**Figure 2. Schematic illustration of the light source and the cylindrical receiver (not to scale)**

hybrid model has already been developed and validated which is called *coupled Monte Carlo/Heat Transfer (cMCHT)* model [15]. The brief description of the cMCHT model is presented here for completeness.

The energy of each primary ray is calculated as:

$$q_p = \frac{q_{in}}{N_{rays}^p} \quad (6)$$

where  $q_p$  represents energy of each primary ray,  $q_{in}$  – the incident energy, and  $N_{rays}^p$  are the total number of primary rays (1 million). The energy of each secondary ray  $q_s$  is calculated:

$$q_s = \frac{q_{rerad}}{N_{rays}^s} \quad (7)$$

The emitted energy from the receiver surface is represented by  $q_{rerad}$  and  $N_{rays}^s$  are total number of secondary rays (1 million). The probability of rays being reflected or absorbed depends on surface reflectivity and estimated using random numbers ( $R_r$ ) between zero and one. The direction of secondary rays are obtained by calculating polar,  $\theta$ , and cone,  $\phi$ , angles given in eq. (8). The paths of rays are tracked until fully absorbed in the receiver or escaped; either from the aperture or the exhaust.

$$\theta = \sin^{-1} \sqrt{R_r}$$

$$\varphi = 2\pi R_r \quad (8)$$

The thermal behavior is calculated using a finite volume based heat transfer model [15]. The energy balance at steady-state for the receiver is given in eq. (9) [15]:

$$q_a + q_e - q_{\text{rerad}} - q_c - q_d - \dot{m}_g c_p (T_g - T_{\text{in}}) = 0 \quad (9)$$

Total energy absorbed in the front plate, back plate, and the cavity is represented by  $q_a$ . The total escaped energy from aperture and exhaust is denoted by  $q_e$ , while  $q_c$  and  $q_d$  represent energy lost by convection and conduction, respectively.  $T_g$  is the temperature of the gas in the receiver, while  $T_{\text{in}}$  is the inlet gas temperature. The mass flow rate and specific heat capacity of the gas are represented by  $\dot{m}_g$  and  $c_p$ , respectively. The equations to calculate absorbed, escaped and emitted energy as well as equations to calculate energy lost by convection and conduction are presented elsewhere [15]. The steady-state energy balance equation to calculate temperature of gas only is:

$$q_c - \dot{m}_g c_p (T_g - T_{\text{in}}) = 0 \quad (10)$$

The components of eq. (4) are re-written for front plate, back plate and cavity of the receiver, and coupled with eq. (5) to obtain fourth order equations [15]. These equations are then, solved simultaneously to obtain temperatures until energy balance is satisfied.

An optical efficiency  $\eta_o$  of the receiver is calculated using eq. (11) which is the ratio of energy absorbed to the energy incident at the receiver:

$$\eta_o = \frac{q_a}{q_{\text{in}}} \quad (11)$$

The optical efficiency is compared with re-radiation losses to obtain optimum aperture(s). The variable aperture sizes are calculated using cMCHT model to maintain constant temperatures for sub-cycle 1-3 for h-SA cycle. Furthermore, power analysis is carried out to investigate power consumptions/savings for variable aperture as compared to selected fixed apertures.

#### *Numerical model input properties*

The input properties of the model are presented in tab. 1 for each sub-cycle of the h-SA cycle. At this point, and for the preliminary assessment of the concept, all reactions have been assumed in the gas phase and the thermo-physical and surface properties of all materials are assumed constant as well as ambient temperature/inlet gas temperature.

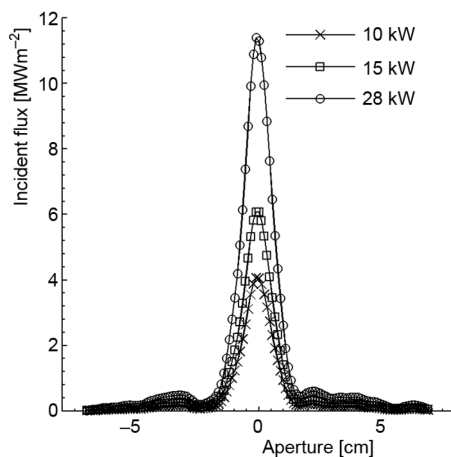
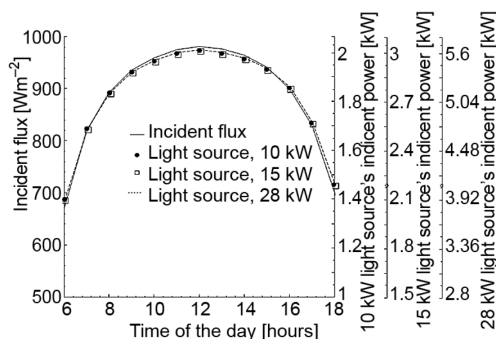
The cavity of the receiver and gas is discretized using 235 control volumes while front and back plate is discretized using 50 and 100 control volumes, respectively. Temperatures of each control volume is calculated using cMCHT model to perform thermal and optical analysis of h-SA cycle.

#### **Results and discussions**

Preliminary studies have been carried out at different power levels of the light sources. It is found that the light source of 10, 15, and 28 kW can achieve desired temperature

**Table 1. Input properties of the cMCHT model**

Properties	Sub-cycle		
	1	2	3
Heat capacity (water-vapor), [ $\text{kJkg}^{-1}\text{K}^{-1}$ ]	2.07	2.17	2.34
Conductivity (water-vapor), [ $\text{Wm}^{-1}\text{K}^{-1}$ ]	0.06	0.07	0.11
Density (water-vapor), [ $\text{kgm}^{-3}$ ]	0.33	0.26	0.20
Conductivity (Inconel), [ $\text{Wm}^{-1}\text{K}^{-1}$ ]	20.9		
Conductivity (insulation), [ $\text{Wm}^{-1}\text{K}^{-1}$ ]	1		
Emissivity	0.85		
Volume flow rate (water-vapor), [ $\text{Lmin}^{-1}$ ]	10		
Stefan-Boltzmann constant, [ $\text{Wm}^{-2}\text{K}^{-4}$ ]	$5.67 \cdot 10^{-8}$		
Inlet gas temperature/ambient temperature, [K]	295		

**Figure 3. Flux distributions of the selected light sources of 10, 15, and 28 kW****Figure 4. Comparison of the incident power variations over the selected day**

of 673 K (for sub-cycle 1), 823 K (for sub-cycle 2), and 1123 K (for sub-cycle 3), respectively. Note, that for this preliminary assessment, all calculations have been conducted based on gas phase reactions which is not the case for reactions (3) and (4). This assumption is quite significant and should be addressed in the detailed study of the receiver. The flux distributions of the selected light sources are shown in fig. 3.

The peak flux of 4.1 MW/m<sup>2</sup> is found for 10 kW light source while corresponding peak fluxes of 15 kW and 28 kW light sources are 6.1 MW/m<sup>2</sup> and 11.4 MW/m<sup>2</sup>, respectively. The incident flux and power variation over the selected day for aperture diameter of 14 cm is calculated and result is shown in fig. 4. The incident flux vs. time is shown on the left ordinate while incident power from light sources of 10, 15, and 28 kW vs. time is shown on first, second, and third right ordinate, respectively.

For 10 kW light source, the incident power changes from 1.4 kW to 2.0 kW (first right ordinate in fig. 4) while incident power changes from 2.1 kW to 3.0 kW for light source of 15 kW (second right ordinate in fig. 4). The corresponding incident power change for 28 kW is in the range of 3.9-5.6 kW (third right ordinate in fig. 4). The difference between maximum and minimum incident power for selected light sources of 10, 15, and 28 kW from 6:00 to 12:00 is found as 611, 916, and 1109 W, respectively. To quantify the effect of power changes on the temperature of the gas, thermal analysis has been carried out for

aperture diameters of 2, 4, 6, 8, 10, 12, and 14 cm. The comparison of optical efficiency and re-radiation losses is presented in fig. 5.

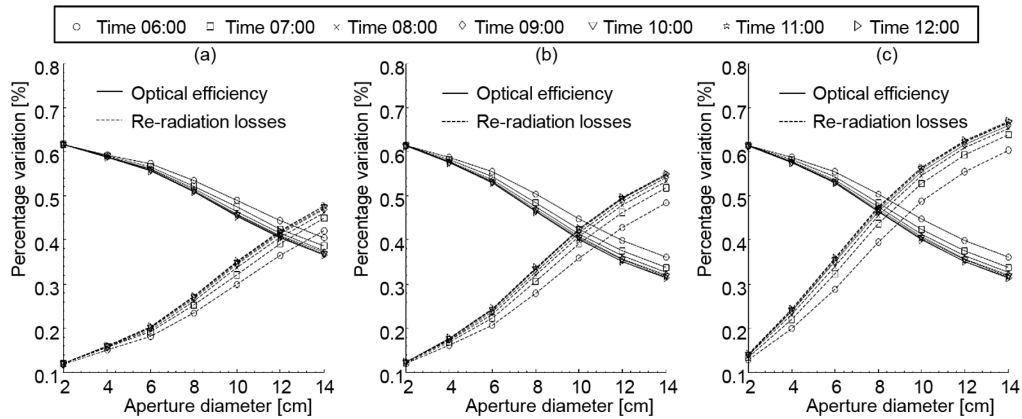


Figure 5. Comparison of optical efficiency and re-radiation losses for (a) sub-cycle 1, (b) sub-cycle 2, (c) sub-cycle 3

The result of this comparison shows that there is no fixed optimum aperture for any sub-cycle. The optimum aperture varies in the range of 11.6-13.8 cm for sub-cycle 1, in the range of 9.2-11.4 cm for sub-cycle 2, and in the range of 7.6-9.4 cm for sub-cycle 3.

Further investigations have been performed to quantify the temperature variation for a fixed optimum aperture (selected from the mentioned range) for each sub-cycle. The result for the selected optimum aperture is presented in tab. 2.

Table 2 shows that a fixed aperture can not maintain constant temperature in the receiver. The maximum to minimum temperature difference for optimum aperture diameters of 12, 10, and 8 cm are ~120, ~150, and ~190 K; for h-SA sub-cycles 1-3, respectively. This variation in temperature can affect the conversion efficiency of the system and may result in affecting process reversibility.

Table 2. Temperature variation of the selected optimum aperture

Time of the day	Sub-cycle 1	Sub-cycle 2	Sub-cycle 3
	Temperature optimum aperture diameter [K]		
	12	10	8
6	658.9	797.7	1075.0
7	720.0	873.9	1172.8
8	748.7	909.2	1217.1
9	764.6	928.6	1241.2
10	772.9	938.6	1253.6
11	778.6	945.5	1262.2
12	780.7	948.1	1265.3
14	774.7	940.7	1256.3
16	752.4	913.8	1222.8
18	672.1	814.3	1096.6
	Mean and standard deviation		
	742.4 ± 44.5	901.0 ± 54.9	1206.3 ± 69.4

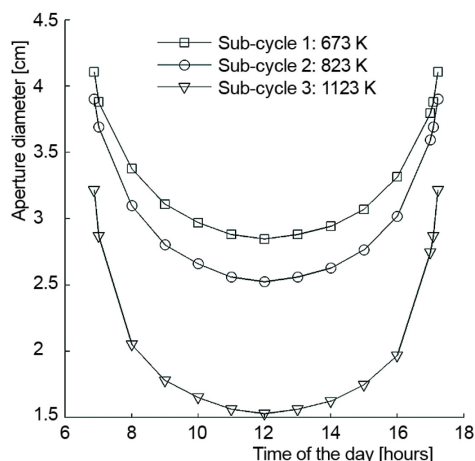


**Figure 6. Variable aperture diameters to maintain constant temperature of 673, 823, and 1123 K for sub-cycles 1, 2, and 3, respectively**

and 26.4 kW per day to maintain constant temperature of 673, 823, and 1123, respectively, for selected sub-cycles. The power consumed by a fixed optimum aperture diameter of 12, 10, and 8 cm for sub-cycle 1, 2, and 3 is found as 20.9, 28.3, and 44.2 kW per day, respectively. This study has shown that the variable aperture saves more than 35% of the power as compared to the respective fixed aperture.

This thermal analysis has shown that the variable aperture has the ability to maintain a constant temperature for solar assisted application like thermochemical water-splitting cycles. The ability of maintaining a constant temperature in a thermochemical application gives an advantage to a process designer to work in a narrow temperature range to maximize conversion efficiency.

## Conclusions

The following conclusions can be drawn from this research.

- The optical and finite volume based coupled Monte Carlo/Heat Transfer model is a suitable tool to perform thermal analysis of multiple step solar driven cycles.
- A fixed optimum aperture applicable to daily variation of the solar irradiance does not exist.
- Variable aperture could maintain a constant temperature for multiple step solar driven cycles.
- Variable aperture in current application consumes less than 65% power than a fixed aperture.

This research is based on a cylindrical receiver with fixed thermo-physical and surface properties along with fixed ambient and inlet gas temperature. Further studies are required to quantify the effect of these variables on thermal behavior of receiver and variable aperture.

## Acknowledgment

Publication of this paper was made possible by a NPRP award [NPRP 6-116-2-044] from the Qatar National Research Fund (a member of The Qatar Foundation). The statements

To counter the effect of temperature variation, variable aperture is investigated, in an effort to maintain a constant temperature for each sub-cycle. The result is presented in fig. 6 which shows that the variable aperture can maintain a constant temperature for each sub-cycle for 10 hours and 22 minutes. More specifically, the variable aperture in the range of:

- 5.7-8.2 cm can maintain a constant temperature of 673 K for sub-cycle 1,
- 5.1-7.8 cm can maintain a constant temperature of 823 K for sub-cycle 2, and
- 3.1-6.4 cm can maintain a constant temperature of 1123 K.

Additionally, the total daily consumed power by variable aperture has also been calculated by integrating the power utilized for maintaining a constant temperature for each sub-cycle. It is found that variable aperture consumes 13.9, 18.3,

made herein are solely the responsibility of the authors. The HPC resources and services used in this work were provided by the IT Research Computing group in Texas A&M University at Qatar. IT Research Computing is funded by the Qatar Foundation for Education, Science and Community Development (<http://www.qf.org.qa>).

## Nomenclature

$c_p$  – heat capacity, [ $\text{Jkg}^{-1} \text{K}^{-1}$ ]  
 $\dot{m}_g$  – mass flow rate, [ $\text{kgs}^{-1}$ ]  
 $N_{\text{ravs}}^p$  – number of primary rays  
 $N_{\text{ravs}}^s$  – number of secondary rays  
 $q_a$  – energy absorbed, [W]  
 $q_c, q_d$  – convection, [W]  
 $q_e$  – energy escaped, [W]  
 $q_{\text{in}}$  – incident energy, [W]  
 $q_p$  – energy of each primary ray, [W]  
 $q_{\text{rerad}}$  – energy re-radiated from the receiver walls, [W]  
 $q_s$  – energy of each secondary ray, [W]  
 $R_r$  – random number

$T_q$  – random number, [K]  
 $T_{\text{in}}$  – temperature of inlet gas, [K]

## Greek symbols

$\eta_0$  – optical efficiency  
 $\theta$  – polar angle, [radians]  
 $\varphi$  – cone angle, [radians]

## Acronyms

cMCHT – coupled finite volume based Monte Carlo/Heat Transfer  
h-SA – hybrid sulfur-ammonia

## References

- [1] Steinfeld, A., Solar Hydrogen Production via a Two-Step Water-Splitting Thermochemical Cycle Based on Zn/ZnO Redox Reactions, *International Journal of Hydrogen Energy*, 27 (2002), 6, pp. 611-619
- [2] Nakamura, T., Hydrogen Production from Water Utilizing Solar Heat at High Temperatures, *Solar Energy*, 19 (1977), 5, pp. 467-475
- [3] Weidenkaff, A., et al., Thermogravimetric Analysis of the ZnO/Zn Water Splitting Cycle, *Thermochimica Acta*, 359 (2000), 1, pp. 69-75
- [4] Moeller, S., Development of a Reactor for the Solar Thermal Production of Zinc from Zinc Oxide for Energy Storage Using Concentrated Solar Radiation (in German), Ph. D. thesis, ETH – Swiss Federal Institute of Technology, Zurich, Switzerland, 2001
- [5] Weidenkaff, A., et al., Direct Solar Thermal Dissociation of Zinc Oxide: Condensation and Crystallisation of Zinc in the Presence of Oxygen, *Solar Energy*, 65 (1999), 1, pp. 59-69
- [6] Palumbo, R. D., Fletcher, E. A., High Temperature Solar Electrothermal Processing – III, Zinc from Zinc Oxide at 1200-1675 K Using a Non-Consumable Anode, *Energy*, 13 (1988), 4, pp. 319-332
- [7] T-Raissi, A., et al., Hydrogen from Solar via Light-Assisted High-Temperature Water Splitting Cycles, *Journal of Solar Energy Engineering*, 129 (2006), 2, pp. 184-189
- [8] Huang, C., et al. Hydrogen Production via UV Photolysis of Aqueous Ammonium Sulfite Solutions, *Proceedings*, WHEC 16, Lyon, France, 2006, Vol. 2, pp. 1010-1018
- [9] Huang, C., et al. Hydrogen Production via Photocatalytic Oxidation of Aqueous Ammonium Sulfite Solutions, *Proceedings*, WHEC 16, Lyon, France, 2006, Vol. 1, pp. 591-599
- [10] Huang, C., et al. Efficiency of the Sulfur-Ammonia Solar Thermochemical Water Splitting Cycle for the Production of Hydrogen, *Proceedings*, WMSCI 2007 – 11<sup>th</sup> World Multi-Conference on Systemics, Cybernetics and Informatics, Jointly with the 13<sup>th</sup> International Conference on Information Systems Analysis and Synthesis, ISAS 2007, Orlando, Fla., US, 2007, Vol. 5, pp. 338-346
- [11] T-Raissi, A., et al., Solar High-Temperature Water-Splitting Cycle with Quantum Boost, *Journal of Solar Energy Engineering, Transactions of the ASME, II.1.2* (2008), 1, pp. 254-259
- [12] Hirsch, D., Steinfeld, A., Solar Hydrogen Production by Thermal Decomposition of Natural Gas Using a Vortex-Flow Reactor, *International Journal of Hydrogen Energy*, 29 (2004), 1, pp. 47-55
- [13] Abanades, S., Flamant, G., Thermochemical Hydrogen Production from a Two-Step Solar-Driven Water-Splitting Cycle Based on Cerium Oxides, *Solar Energy*, 80 (2006), 12, pp. 1611-1623
- [14] Kodama, T., et al., Flux Measurement of a New Beam-Down Solar Concentrating System in Miyazaki for Demonstration of Thermochemical Water Splitting Reactors, *Energy Procedia*, 49 (2014), Dec., pp. 1990-1998

- [15] Sarwar, J., *et al.*, Experimental and Numerical Investigation of the Aperture Size Effect on the Efficient Solar Energy Harvesting for Solar Thermochemical Applications, *Energy Conversion and Management*, 92 (2015), Mar., pp. 331-341
- [16] Jubb, A., Solar Heat Aperture Control Apparatus, Rolls-Royce Limited, Patent No. US4222367 A, 1980
- [17] Abdulla, S., *et al.* Design, Manufacturing and Testing of a Camera-Like Aperture Mechanism for a Solar Reactor, *Proceedings*, ASME 2011 International Mechanical Engineering Congress and Exposition. Denver, Coll., USA, 2011, Vol. 3, pp. 305-319
- [18] Ozalp, N., *et al.*, A Smart Solar Reactor for Environmentally Clean Chemical Processing, *Chemical Engineering Transactions*, 25 (2011), Jan., pp. 989-994
- [19] Wu, Z., *et al.*, Three-Dimensional Numerical Study of Heat Transfer Characteristics of Parabolic Trough Receiver, *Applied Energy*, 113 (2014), Jan., pp. 902-911
- [20] Fuqiang, W., *et al.*, Thermal Performance Analysis of Porous Medium Solar Receiver with Quartz Window to Minimize Heat Flux Gradient, *Solar Energy*, 108 (2014), Oct., pp. 348-359
- [21] Xiao, X., *et al.*, Experimental and Numerical Heat Transfer Analysis of a V-Cavity Absorber for Linear Parabolic Trough Solar Collector, *Energy Conversion and Management*, 86 (2014), Oct., pp. 49-59
- [22] Sarwar, J., *et al.*, Description and Characterization of an Adjustable Flux Solar Simulator for Solar Thermal, Thermochemical and Photovoltaic Applications, *Solar Energy*, 100 (2014), Feb., pp. 179-194
- [23] \*\*\*, Solar Radiation Research Laboratory, Daily Plots and Raw Data Files, [http://www.nrel.gov/midc/srrl\\_rsp2/](http://www.nrel.gov/midc/srrl_rsp2/)